Environmental Science & Technology

pubs.acs.org/est

Article

Spatiotemporal Characteristics and Driving Factors of Black Carbon in Augsburg, Germany: Combination of Mobile Monitoring and Street View Images

Xiansheng Liu, Xun Zhang,* Jürgen Schnelle-Kreis,* Gert Jakobi, Xin Cao, Josef Cyrys, Lanyan Yang, Brigitte Schloter-Hai, Gülcin Abbaszade, Jürgen Orasche, Mohamed Khedr, Michal Kowalski, Marcus Hank, and Ralf Zimmermann

Cite This: https://dx.doi.org/10.1021/acs.est.0c04776

Read Online

ACCESS | Metrics & More | Article Recommendations | Supporting Information

ABSTRACT: The study investigates the spatial pattern of black carbon (BC) at a high spatial resolution in Augsburg, Germany. Sixty two walks were performed to assess the concentrations of equivalent black carbon (eBC), ultraviolet particulate matter (UVPM), and equivalent brown carbon (eBrC) in different seasons and at different times of the day with a mobile platform (i.e., trolley). Along with BC measurements, images of street microenvironments were recorded. Meteorological parameters, including temperature, relative humidity, and wind speed, were monitored. The BC concentrations showed significant spatial heterogeneity and diurnal variations peaking in the morning and at night. The highest BC concentrations were observed near dense traffic. The correlations between BC and street views (buildings, roads, cars, and vegetation) were weak but highly significant. Moreover, meteorological factors also influenced the BC concentration. A model based on street view images and meteorological data was developed to examine the driving factors of the spatial variability of BC concentrations at a higher spatial resolution as different microenvironments based on traffic density. The best results were obtained for UVPM and eBC (71 and 70% explained variability). eBrC (53%), to which other sources besides road traffic can also make significant contributions, is modeled less well.

1. INTRODUCTION

Since the 20th century, air pollution has been one of the major environmental problems in metropolitan areas,[1−3] with black carbon (BC), an optically absorbing substance, contributing less than 5−10% to the total mass concentration of particulate matter ($PM_{2.5}$).[4] Severely, it has different toxicities to sensitive targets in the human body, such as the lungs, the body's main defense cells, and even systemic blood circulation.[5−7] In 2012, the International Agency for Research on Cancer (IARC) classified BC containing diesel soot carcinogenic to humans.[8] Meanwhile, Janssen et al. (2011) found that BC can be used as a valuable air quality indicator for assessing the health risks of traffic-related air pollution.[9] Hence, in this study, the spatial characteristics and driving factors of black carbon were studied.

The monitoring of air quality by high-quality stationary measurements, as usually performed in official monitoring networks, has limitations when investigating the spatial variability of human exposure. Therefore, mobile monitoring[10,11] has been widely applied for the collection of real-time air quality measurements to assess local air quality and air pollutant exposures. This method can improve the temporal and spatial resolution of measurement data of in the urban environment and enables the collection of data such as the traffic-related air pollutant concentrations and driving factors in microscale road sections.[12] Mobile measurements are,

Received: July 20, 2020
Revised: November 26, 2020
Accepted: November 30, 2020

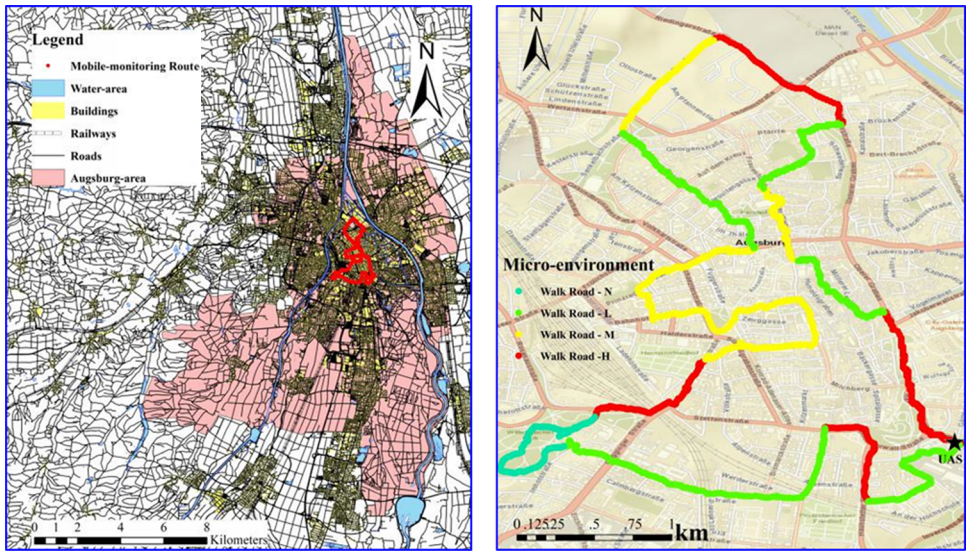

Figure 1. Location and road of the sampling sites in Augsburg, Germany. Left: main urban area of Augsburg (Data/Maps Copyright 2018 Geofabrik GmbH and OpenStreetMap contributors), right: sampling route map, different colors represent different traffic densities in the microenvironments; red, high traffic roads (H_Traffic); yellow, medium traffic roads (M_Traffic); green, low traffic roads (L_Traffic); blue, park area (N_Traffic); start and end point, UAS (University of Applied Sciences).

therefore, favorably used in human exposure studies to quantify individual exposures and to demonstrate the importance of exposure differences in different microenvironments.[13−16] For example, Bassok et al. (2010) used a portable detector to measure the BC concentration of traffic sources in the Seattle International District and discussed the spatial and temporal distributions of the BC concentration on a street scale.[17]

Changes in the air quality in the city are not only related to the distribution of vehicle emissions but also to the urban development, street characteristics, street location, and land use types.[18−22] Hankey et al. (2015) used bicycle-based, mobile measurements during rush hour in Minneapolis, USA to build land-use regression models for particulate concentrations.[16] Apte et al. (2017) equipped Google Street View vehicles with a fast-response pollution measurement platform and repeatedly sampled every street in a 30 km^2 area of Oakland, CA, developing the largest urban air quality data set of its type.[23] Messier et al. (2018) mapped spatial air quality patterns using an unusually rich data set of repeated mobile air quality measurements collected with specially equipped Google Street View cars.[24] Hankey and Marshall (2015) studied the regression models of video-derived traffic counts and particle concentrations.[25] They used the counts of each vehicle type (i.e., passenger cars, trucks, and buses) as independent variables in the regression model to estimate the particulate matter concentration. Liang et al. (2017) used remote sensing images to obtain urban sky, trees, and architectural landscape factors to study the correlation between urban environment and air quality.[26] Therefore, the use of images to assess air pollution is potentially feasible and desirable. However, the previous models, such as Google Street View and remote sensing images, have certain limitations due to the detailed information that may not be obtained in small scales. Nowadays, the street view images provide an excellent option acquired within urban street canyons and provide a human-centered view of the built environment.[27] However, it remains unclear how to develop street view images to predict air pollutants.

In this study, we used portable instrument-based microair pollution monitoring devices to monitor the actual exposure level of black carbon pollution to the population in Augsburg and at the same time to collect the street view images to predict air pollutants. The primary goals of the present study were (1) to provide the spatiotemporal variability of BC in urban street environments with a high spatial and temporal resolution; and (2) to develop street BC models based on street view images for predicting spatial patterns in exposure to BC for Augsburg, Germany. Our approach is innovative because it investigates a street view image model to predict BC exposure as experienced by a pedestrian in an urban environment.

2. MATERIALS AND METHODS

2.1. Study Area. The mobile measurements were carried out in Augsburg, Germany. It is the third largest city in Bavaria (after Munich and Nuremberg) with about 300 000 inhabitants and about 660 000 residents in its metropolitan area. The mean annual temperature and precipitation are 13.2 °C and 767 mm, respectively. It has an oceanic climate that tends to clouds with precipitation.

This investigation was part of the Smart Air Quality Network (https://www.smartaq.net/) project. A fixed walking path within the center of the city was determined. Wherever possible, the walks were carried out on the right side of the road due to people's daily habits (driving and walking on the right side in Germany) and walked repeatedly in the course of the investigations. The route started from Augsburg University of Applied Sciences and passed through different types of land use to ensure that the selected path runs across different microenvironments and may be representative for the entire city. It is approximately 14 km long (Figure 1). The average walking time for the entire route was approximately 3 h.

We divided the monitoring route into four microenvironment classes, high traffic roads (H_Traffic, average 500−1000 vehicles/h), medium traffic roads (M_Traffic, average 200−500 vehicles/h), low traffic roads (L_Traffic, average 1−200 vehicles/h), and park area (N_Traffic, average 0 vehicles/h)

https://dx.doi.org/10.1021/acs.est.0c04776
Environ. Sci. Technol. XXXX, XXX, XXX−XXX

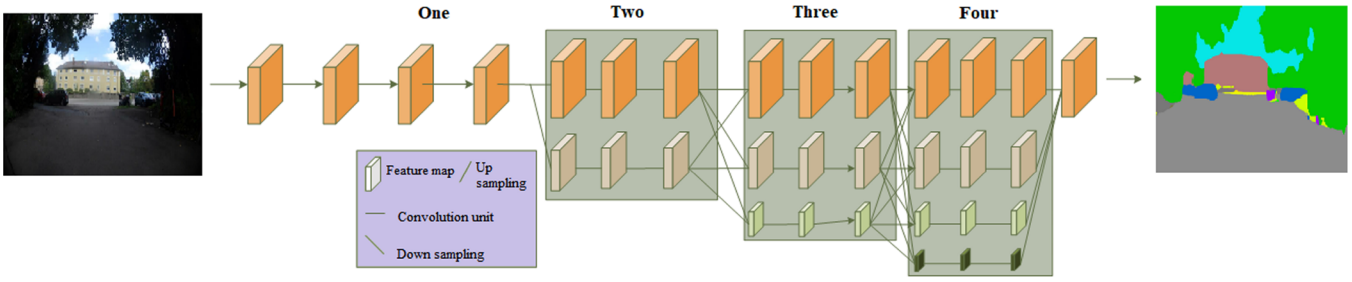

Figure 2. Schematic diagram of sample segmentation image processed by the HRnet model.

according to the actual traffic density examined during the daytime, determined from the traffic flow observed by the street views.

2.2. Sampling Campaign. All walks along the route were conducted on weekdays from August 2018 to June 2020, with clear skies (i.e., nonrainy days) and calm winds. The detailed description for each sampling run is illustrated in Table S1. Mobile platforms were built on a trolley, and air-monitoring devices were installed in a box attached to the trolley. It was equipped with a GPS (GPSMAP 64s, Garmin, USA) to register the measurement location at 1 s resolution, and a point-of-view (POV) camera (TG-Tracker, Olympus, Japan) to record the street view images at 5 s resolution. Comparative measurements of the MicroAeth MA200 to measurements carried out with a stationary instrument (Magee, model AE33, Aerosol Co. Slovenia) were made between the individual walks.

BC concentrations were measured by a multiwavelength Aethalometer (microAethalometer, MA200, AethLabs, USA) with a time resolution of 10 s to avoid excessive noise of the BC signal. The Aethalometer measures the light attenuation through a filter tape at five wavelengths, while the filter is continuously collecting aerosol at a flow rate of 150 mL/min. Measurement at 880 nm is defined as the concentration of BC, while measurement at 375 nm is interpreted as ultraviolet particulate matter (UVPM). The brown carbon (BrC) is the fraction of carbonaceous aerosols, excluding black carbon, which absorbs light primarily at the low visible wavelengths and the near ultraviolet range, expressed as the difference eBrC = UVPM (375 nm) − eBC (880 nm).[28−31]

2.3. Meteorological Data Monitoring. The meteorological parameters including air temperature (T), relative humidity (RH), and wind speed (WS) were measured by a monitoring station in Augsburg located in the urban background on the campus of the University of Applied Sciences (UAS), which is operated jointly since 2004 by the Helmholtz Zentrum München (German Research Center for Environmental Health, Munich) and Environmental Science Center, University Augsburg.[32]

2.4. Postprocessing of BC Data. The Aethalometer measurement in environments with low BC concentrations and/or at high time resolution triggers for negative value detection due to the instrumental noise and changing relative humidity conditions.[33] Negative values frequently contain valid information that is required for postprocessing or smoothing the data over a long interval; hence, the removal of negative values may be detrimental to a dataset.[34]

For postprocessing data, MA200 microAeth users can upload their data file to AethLabs platform (http://www.aethlabs.com) and apply "postprocessing tools" to smoothen their data. Whereas various different algorithms are available in this process. The commonly applied time-adaptive noise reduction method is centered moving average (CMA), which is used to build the underlying trends of a time series.[35] Unlike a simple moving average, there is no shift or group delay in the data using the CMA. Therefore, the CMA was chosen in this study. The comparison between original BC measurements and CMA averaging seven data points is illustrated in Figure S1. The denoising results show that the CMA can reduce negative anomalies that occur in the raw BC data. In our study, comparative measurements of the MicroAeth MA200, which were used in the trolleys to measurements carried out with a stationary instrument (Magee, model AE33, Aerosol Co. Slovenia), were simultaneously made between the individual walks (see details in the Supporting Information, Section 1). The comparison showed very good agreement of the results (Pearson's r = 0.977 and 0.933 and R^2 = 0.955 and 0.871 for UVPM and eBC, respectively, Figure S2) independent on time of day and season.

2.5. BC Modeling Using the Street View Image Model. *2.5.1. Street View Image Model.* In order to quantify the composition of the surface types that pedestrians experience in the street canyon, the method of deep learning was used, which can create a unique description of the urban form and composition as experienced by a pedestrian in the street and is, therefore, more relevant to the human experience of cities compared to planar bird's eye views from satellite data. In this study, the images are captured by a camera in the daylight walking, and the street view images were mainly segmented into five types: buildings, roads (including parking cars), vegetation, cars (only cars in traffic), and sky.

2.5.2. The Semantic Segmentation Algorithm of Street Scenes Based on the HRnet Model. To obtain the surrounding environment elements of the current location, the street view image is segmented into some categories to obtain the proportions area of different elements of the scene in the current image. In this study, the high-resolution network (HRnet) is selected as the main model structure for semantic segmentation.[36] As a standard backbone network, the HRnet network structure has obtained good results in image classification, target detection, and semantic segmentation. Furthermore, the previous studies proved that HRnetV2, one version of HRnet, has a good effect in the cityscape public dataset, and the average intersection ratio (mIoU) obtained by the model in the verification set is higher than that of classic networks such as Unet, PSPNet, and DeepLabv3+.[37−41] Because our street view images are classified into categories and image scenes from the cityscape dataset, they are both very similar to the semantic segmentation of street view images. So this study adopted the HRnetV2 model as the street view image segmentation network.

https://dx.doi.org/10.1021/acs.est.0c04776
Environ. Sci. Technol. XXXX, XXX, XXX−XXX

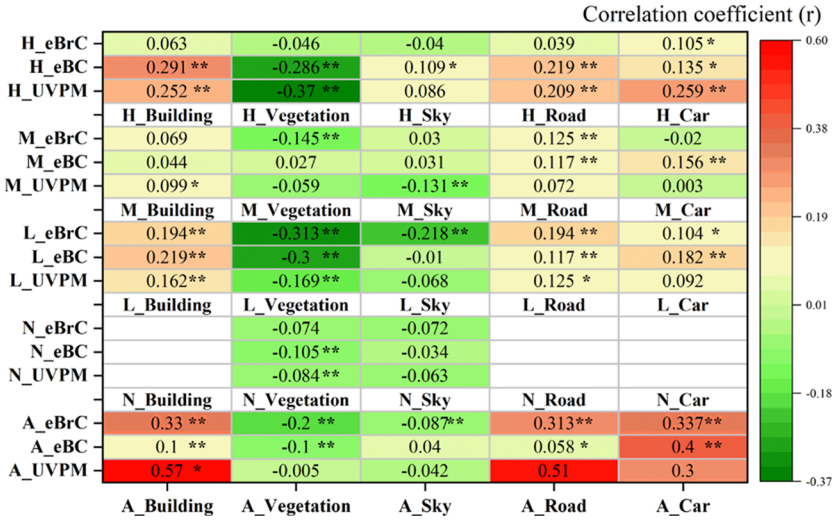

Figure 3. Correlation matrix of measured compounds in different traffic volumes (A, all roads; N, no traffic volume (park area); L, low traffic volume; M, middle traffic volume; H, high traffic volume, *p < 0.05, **p < 0.01, and white bands represent nonsense).

As shown in Figure 2, the HRnet network structure can be divided into four parts with minor modification.[36] Briefly, the first part is composed of four bottleneck structural blocks, and the second, third, and fourth parts are all composed of structural blocks of residual units. After the transmission of the first part is completed, two branches are generated through two convolutional layers of different sizes and transmitted to the second part in parallel. On the branch, four structural blocks of residual units are serially connected and transmitted. When transmitting to the third part, a new low-resolution branch is generated through the convolutional layer again, and then the feature layers of the three branches are up-sampled and down-sampled. The sampling methods are combined and transmitted to the fourth part. Similarly, in the fourth stage, the data is transmitted in parallel on the four branches, and after the transmission is completed, it is all merged to the original resolution through up-sampling. Finally, the feature layer is output through the convolutional layer. In this study, we used the pytorch1.3 version, with four GTX 1080ti GPUs to pretrain the network, batch size is 12, and training round epochs is 500.

2.5.3. Model Accuracy Evaluation Method. The accuracy evaluation of the model can reflect the fitting effect and the error of the model. In this study, we used the cross-validation (CV) method that used 70% of the monitoring data as the training data, and the 10-fold CV method to estimate the accuracy of the model.[42] This method can balance the deviation and variance of the model. By assessing the closeness between the simulation result of the verification set and the actual observation value, the simulation accuracy of the model is reflected. The evaluation indicators used in this study include the correlation coefficient (R), the root mean square error (RMSE), the mean absolute error (MAE), and the fitting index (index of agreement, IA). Where R represents the model, the fitting effect of RMSE and MAE represent the deviation between the predicted value and the actual value, and IA represents the consistency between the predicted value and the actual value.

2.5.4. Random Forest Algorithm. One of the challenges derived by regression-based street view image models is difficulty to capture nonlinear relationships and complex interactions. Random forest can resist and overcome these problems.[43,44] To predict the urban black carbon concentrations, the random forest was selected for the street view image model. We used the default setting from the package scikit-learn. A bivariate correlation analysis was used in this study to extract the target factors required for modeling, and the concentrations of UVPM, eBC, and eBrC in the training set and the corresponding target factors were used as data for the random forest regression method. In order to express the simulation accuracy of the random forest optimization method, the fitting indices of the support vector machine (SVM) optimization method[45] and the multiple linear regression (MLR) method[46] were also calculated and compared.

3. RESULTS AND DISCUSSION

3.1. Spatiotemporal Variations of Median Black Carbon Concentrations across Street Microenvironments. Because the median is a more representative central tendency measure than the mean,[47] the study preferred to use the median to investigate the spatial variation of BC concentrations. Figure S3 shows the aggregated median UVPM, eBC, and eBrC concentrations for each 15 m distance along the route. The observed median BC concentrations in different microenvironments exhibited substantial spatial heterogeneity, with the lowest values in the park environment (N_traffic) and the highest in the H_traffic environment (see details in the Supporting Information, Section 2.1). For eBC, the averages in the busier roads were obviously higher than those of others (p < 0.05 with ANOVA method) (Figure S4). The areas with highest traffic intensities, particularly on crossroads, showed high BC concentrations (Figure S3), e.g., the crossroads of P1 (10.3, 10.0, and 0.34 $\mu g/m^3$), P2 (11.6, 10.4, and 1.20 $\mu g/m^3$), and P3 (10.88, 9.38, and 1.50 $\mu g/m^3$). Meanwhile, based on the Spearman correlation, the three parameters have weak to strong significant correlations, as following UVPM *versus* eBC (0.917, p < 0.01); UVPM *versus* eBrC (0.642, p < 0.01); and eBC *versus* eBrC (0.361, p < 0.01).

Generally, high levels of pollutant concentrations occur in areas with the largest traffic volumes. These regions are hotspots for eBC concentrations. It could be concluded that the direct emissions from the traffic could be an important source for BC in Augsburg. On the other hand, in the central business district, the main means of transportation are trams

https://dx.doi.org/10.1021/acs.est.0c04776
Environ. Sci. Technol. XXXX, XXX, XXX−XXX

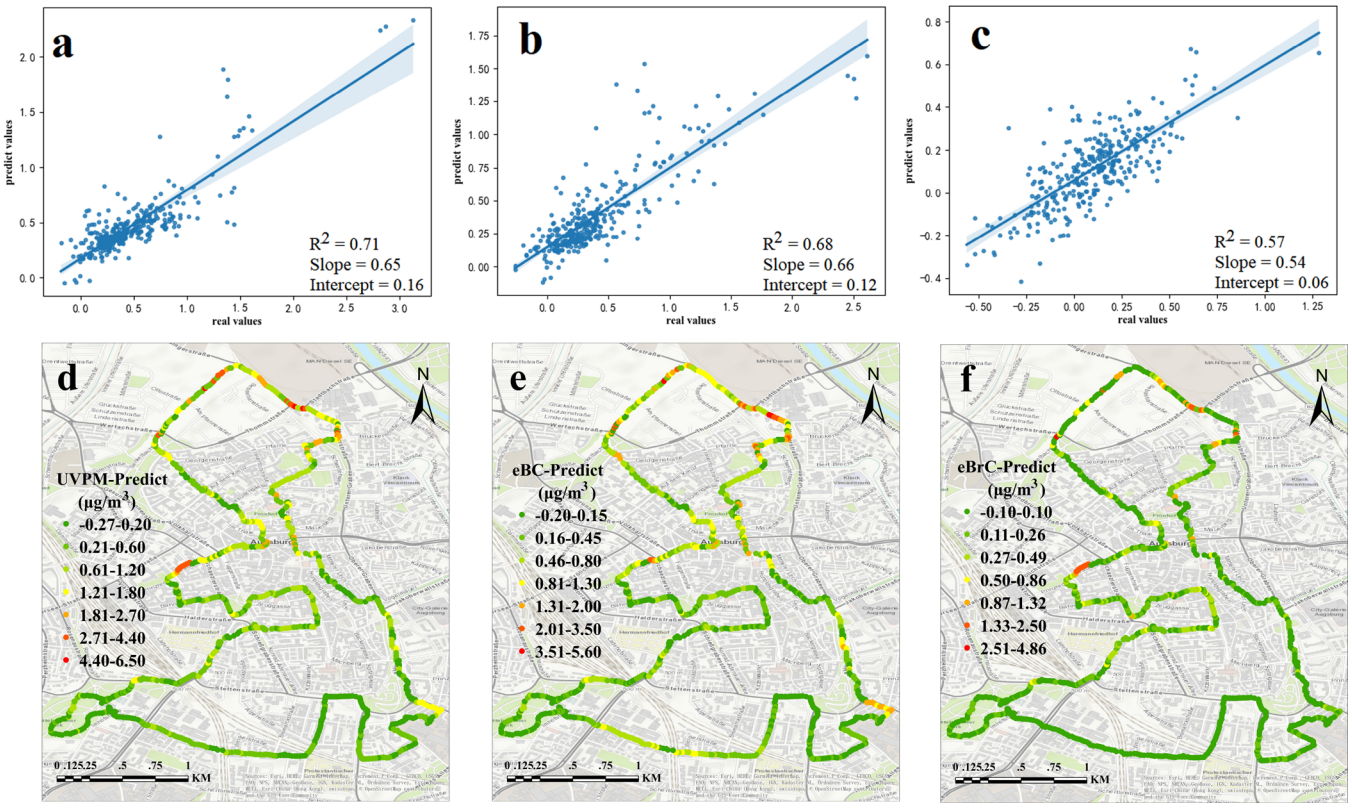

Figure 4. The random forest method and prediction of the spatial distribution of air pollutants (a–c) random forest optimization method for UVPM, eBC, and eBrC; and (d–f) spatial distribution for prediction exposure to UVPM, eBC, and eBrC).

and natural gas-operated buses. In other regions, cars are the mainstay. Especially on some main roads, high-emission vehicles like heavy-duty trucks are common. Targino et al. (2016) pointed out that the pollution concentrations were positively correlated with traffic loads and observed a strong relationship between eBC concentrations at intersections managed by traffic signals and the number of heavy-duty diesel vehicles.[48] Boogaard et al. (2011) averaged the ratio of the pollutant concentration of multiple streets (10 000–18 000 vehicles/day) to the background and found that the street eBC concentration was higher than the background.[49] In summary, the highest eBC concentrations in Augsburg were near traffic roadways, especially at street crossings and traffic lights.

In comparison with temporal variations, the differences in UVPM, eBC, and eBrC concentrations measured in four seasons were generally significant ($p < 0.05$, Figure S5). In spring, summer, autumn, and winter, the variation trends of the three air pollutants were similar. The median concentrations of UVPM, eBC, and eBrC are respectively 3.86, 3.55, and 2.68 times higher in winter than that in spring. This can be attributed to seasonal differences in meteorological conditions and emission sources (Figure S5, details in the Supporting Information, Section 2.2). In addition, the diurnal variation of BC was strikingly sharp in the morning peaks and late afternoon to late night. The maximum concentrations around midnight were 4.2, 3.7, and 6.8 times higher than those observed in the afternoon for UVPM, eBC, and eBrC, respectively (Figure S6, details in the Supporting Information, Section 2.3).

3.2. Association of BC Concentrations and Potential Driving Factors. The correlation analysis between the BC concentration and driving factors and the streetscape images was observed. As shown in Figure 3, the correlations between street scene (buildings, roads, cars, and vegetation) and UVPM, eBC, and eBrC carbon are weak but highly significant. Similarly, Choi et al. (2016) found that the block-scaled ultrafine particle (UFP) concentrations highly depend on the built environment and surface turbulence.[22] Black carbon has a similar character to UFP and is related to the built environment. Open blocks may be one of the reasons and give the benefit to the dispersion of pollutants, while high and narrow buildings reduce the dispersion of pollution from the upper wind. Peters et al. (2013) selected two fixed roads in the cities of Antwerp and Mol in Belgium to test the UFP.[47] The results also showed that the daily concentration of UFP changes closely with the traffic density flow and the structure of the street. Pan et al. (2013) also found that the dispersion of pollutants in urban canopies is indirectly affected by the shape of the buildings.[50] The impact of automobiles on pollutants is mainly caused by automobile exhaust, which is the main source of black carbon.[51] The relationship between vegetation and black carbon is inversely related because the urban forest system can store and capture dust in the air,[52] which purifies the black carbon concentration. More than that, meteorological factors (T, RH, and WS) also influence the BC concentrations in the urban area, which was observed and found in the current and previous studies[34] (see details in Section 3, Supporting Information).

For different microenvironments, the correlation between street scene indicators and the three air pollutants is slightly different, caused by the different proportions of street scenes in different microenvironments (Figure 3).[53] Most of the vegetation is found in the park area, resulting in the low concentrations of UVPM, eBC, and eBrC. In the micro-

https://dx.doi.org/10.1021/acs.est.0c04776
Environ. Sci. Technol. XXXX, XXX, XXX–XXX

environment of medium traffic flow, the correlation between UVPM and the building is very weak but still significant. However, the correlations between eBC, eBrC, and the building are not significant. A wider range in the proportion of buildings may be the reason for this observation.

3.3. Evaluation and Prediction of UVPM, eBC, and eBrC Concentrations. *3.3.1. The Fitting Effects of Random Forest (RF) and Its Application.* The scatterplots of the predicted and observed values of the UVPM, eBC, and eBrC for RF methods are shown in Figure 4a−c), and the relationship between each predictor and the three pollutants are shown in Figure S8. The scatterplots of the predicted and observed values of the UVPM, eBC, and eBrC for SVM and MLR are shown in Figure S9. In the same sampling, 70% of the monitoring data was selected as the training data, and the 10-fold CV method was used to estimate the accuracy of the method, where the data set is randomly separated to 10 partitions with equal-sized folds. The algorithm is trained using ninefolds and repeated 10 times. We performed the sampling with replacement, suggesting that every fold could be used as the validation set exactly once. As a result, the correlation coefficient (R), root mean square error (RMSE), mean absolute error (MAE), and fitting index (IA) of the UVPM (eBC and eBrC) prediction method are shown in Table S2. Based on the R^2 and IA, the RF method is superior to the other two types of methods, and it performs better in the Augsburg black carbon aerosol simulation: concentration space simulation. This is because the main advantage of random forest is that ability to capture the complex and nonlinear relationship between predictor variables and results with small-scale training data.[54] Moreover, the effects of the SVM and the MLR method fitting are not suitable for this study (Table S2), as both applications will lead to an obvious overfitting. If random forests can indeed capture more patterns based on street view images, they may be more accurate predictors of pollutant concentration.[54] Thus, to determine the dominant factors of the model, the weight of each factor was analyzed based on the RF method, and we found that the relative humidity has a greater influence for UVPM, eBC, and eBrC. In addition, other dominant factors are wind speed and temperature for UVPM, temperature and vegetation for eBC, and vegetation for eBrC.

Based on the prediction models of three pollutants established in this study, we have spatialized the model prediction, as shown in Figure 4d−f. The predicted concentrations of the three pollutants (UVPM, eBC, and eBrC) and the actual traffic flow in different microenvironments are mainly consistent (high traffic flow and high pollutant concentration), which further illustrate the applicability of the model built in this study. It is worth noting that the RF method is the best for UVPM and eBC prediction; however, for eBrC, it is poor, which may be caused by the source of eBrC. Previous studies have shown that wood combustion in Germany is frequently used for leisure.[55] We therefore estimated that eBrC can be associated with smoke from the smoldering phase of wood combustion and leisure. However, during the sampling process, the camera did not collect relevant information (e.g., wood combustion).

3.3.2. Street View Image Model and Its Comparison with Other Models. The most widely used models for spatial distribution simulation include spatial interpolation, remote sensing inversion, atmospheric diffusion models, land use regression (LUR), and hybrid models of the latter.[56] Atmospheric diffusion models, LUR, and hybrid models can provide pollution estimates on comparable spatial scale as our model. Hence, we very briefly discuss advantages and disadvantages of these models compared to our street view image-based approach.

If the atmospheric diffusion model (e.g., MISKAM and computational fluid dynamics (CFD) model)[57] is used to simulate black carbon concentration in the microscale environment, the input data required in the model are terrain, meteorological data, pollution source data (point source/area source), and emission factors of relevant sources as well as activity pattern (time-dependent emission strengths). A major advantage is their ability to calculate the pollutant concentration of various sources and integrate simple and complex terrain. Yet their use is improper for the modeling in low wind speeds,[57] where the wind speed inside Augsburg urban area is relatively low, especially in winter and spring (Table S1). Depending on time and spatial resolution of input data, results are comparable in spatiotemporal resolution to our model. However, for the calculation of pollutant concentrations with high spatial resolution (e.g., 10 m grid width),[57] on the one hand, source information in similar resolution is needed, which is usually not available. For the model calculations, therefore, assumptions about the sources (i.e., emission position and intensity and activity pattern) must often be used. On the other hand, the calculations require high computing power or long computing times, especially at high spatial resolution. Regarding LUR, the input data required in this model are representative concentrations of atmospheric pollutants determined at several monitoring sites and land use data, road traffic flow, meteorological data, and other factors potentially influencing concentrations near the monitoring points.[58] Moreover, this model is a cost-effective tool for predicting spatial variability in ambient air pollutant concentrations with high resolution.[16] Usually, input data for LUR modeling is sufficient to achieve similar spatial resolution like our approach for the BC estimation. However, results from LUR modeling are usually time-invariant. In addition, the selection of the number of monitoring sites and how to determine the contribution ability of different elements to pollutants and the distance between them needs to be further explored and discussed.[58] In order to further prove the superiority of our model, we compare LUR with our model more specifically (see details in the Supporting Information, Section 4) in the supporting material, and the results show that the R^2 of LURF (0.33−0.64) in different buffers are lower than that in our street view image model (0.53−0.71).

Hybrid models that combine elements of LUR and dispersion models provide the opportunity to exploit the advantage of the abovementioned techniques while mitigating their shortcomings.[59] When the necessary data support is lacking, advanced dispersion may perform poorly. In this case, the LUR model result can be used as input dispersion modeling.[56] As a result, the hybrid model explained more variance than other compared models in the study. However, it may require more complex analysis than a single model, and the lack in uniformity of the verification model will make it difficult to compare with reviewed models.[60]

The street view image model proposed in this study can provide a prediction of UVPM, eBC, and eBrC concentration levels with high accuracy and efficiency. This model can effectively overcome some shortcomings of other models in predicting air pollution, such as, it is applicable in the low wind

https://dx.doi.org/10.1021/acs.est.0c04776
Environ. Sci. Technol. XXXX, XXX, XXX−XXX

speed level, easily identifying the hotspot and simple analysis. In addition, the model has strong timeliness, which can capture the actual conditions of the daytime environment. In the future, street view image model may prospect to develop in different areas or even areas that cannot be accessed by air quality monitoring equipment. The concentrations of UVPM, eBC, and eBrC can be estimated by using street view images combined with meteorological factors in the area. Moreover, street view images can easily obtain the types of features with highly detailed information. However, the street view image model still has certain limitations, such as meteorological data that is not measured along the path (see in the Supporting Information, Section 5), and further improvements are still needed in the future.

■ ASSOCIATED CONTENT

Supporting Information

The Supporting Information is available free of charge at https://pubs.acs.org/doi/10.1021/acs.est.0c04776.

Comparative measurement of MicroAeth MA200, spatiotemporal variations of median black carbon concentrations in Augsburg, meteorological effects on BC concentrations, comparison LURF and a street view image model, and limitations in BC estimation; descriptions of the meteorological conditions (Table S1); comparison of random forest fitting effects (Table S2); comparison of land use random forest (Table S3); comparison between original BC measurements and corrections (Figure S1); comparative measurements of the MicroAeth MA 200 with AE33 (Figure S2); spatial distribution of the median UVPM, eBC, and eBrC exposure concentrations (Figure S3); box plots of median concentrations of UVPM, eBC, and eBrC in different microenvironments (Figure S4); comparison of UVPM, eBC, and eBrC concentrations among different seasons (Figure S5); diurnal variations of mean UVPM, eBC, and eBrC concentrations in Augsburg (Figure S6); correlation matrix of measured compounds in different traffic volumes (Figure S7); scatter diagrams of relationship between each predictor and the three pollutants (Figure S8); support vector machine optimization and multiple linear regression method (Figure S9); and land use random forest model in different buffers for UVPM, eBC, and eBrC (Figure S10) (PDF)

■ AUTHOR INFORMATION

Corresponding Authors

Xun Zhang − *Beijing Key Laboratory of Big Data Technology for Food Safety, School of Computer Science and Engineering, Beijing Technology and Business University, Beijing 100048, China;* orcid.org/0000-0002-5502-2974; Email: zhangxun@btbu.edu.cn

Jürgen Schnelle-Kreis − *Joint Mass Spectrometry Center, Cooperation Group Comprehensive Molecular Analytics, Helmholtz Zentrum München, German Research Center for Environmental Health, Neuherberg 85764, Germany;* Email: juergen.schnelle@helmholtz-muenchen.de

Authors

Xiansheng Liu − *Joint Mass Spectrometry Center, Cooperation Group Comprehensive Molecular Analytics, Helmholtz Zentrum München, German Research Center for Environmental Health, Neuherberg 85764, Germany; Joint Mass Spectrometry Center, Chair of Analytical Chemistry, University of Rostock, Rostock 18059, Germany;* orcid.org/0000-0002-0228-5551

Gert Jakobi − *Joint Mass Spectrometry Center, Cooperation Group Comprehensive Molecular Analytics, Helmholtz Zentrum München, German Research Center for Environmental Health, Neuherberg 85764, Germany*

Xin Cao − *Joint Mass Spectrometry Center, Cooperation Group Comprehensive Molecular Analytics, Helmholtz Zentrum München, German Research Center for Environmental Health, Neuherberg 85764, Germany; Joint Mass Spectrometry Center, Chair of Analytical Chemistry, University of Rostock, Rostock 18059, Germany*

Josef Cyrys − *Institute of Epidemiology II, Helmholtz Zentrum München, German Research Center for Environmental Health, Neuherberg 85764, Germany; Environmental Science Center (WZU), University of Augsburg, Augsburg 86159, Germany*

Lanyan Yang − *Beijing Key Laboratory of Big Data Technology for Food Safety, School of Computer Science and Engineering, Beijing Technology and Business University, Beijing 100048, China*

Brigitte Schloter-Hai − *Joint Mass Spectrometry Center, Cooperation Group Comprehensive Molecular Analytics, Helmholtz Zentrum München, German Research Center for Environmental Health, Neuherberg 85764, Germany*

Gülcin Abbaszade − *Joint Mass Spectrometry Center, Cooperation Group Comprehensive Molecular Analytics, Helmholtz Zentrum München, German Research Center for Environmental Health, Neuherberg 85764, Germany*

Jürgen Orasche − *Joint Mass Spectrometry Center, Cooperation Group Comprehensive Molecular Analytics, Helmholtz Zentrum München, German Research Center for Environmental Health, Neuherberg 85764, Germany*

Mohamed Khedr − *Joint Mass Spectrometry Center, Cooperation Group Comprehensive Molecular Analytics, Helmholtz Zentrum München, German Research Center for Environmental Health, Neuherberg 85764, Germany; Joint Mass Spectrometry Center, Chair of Analytical Chemistry, University of Rostock, Rostock 18059, Germany*

Michal Kowalski − *Institute of Epidemiology II, Helmholtz Zentrum München, German Research Center for Environmental Health, Neuherberg 85764, Germany*

Marcus Hank − *GRIMM Aerosol Technik Ainring GmbH & Co., Ainring 83404, Germany*

Ralf Zimmermann − *Joint Mass Spectrometry Center, Cooperation Group Comprehensive Molecular Analytics, Helmholtz Zentrum München, German Research Center for Environmental Health, Neuherberg 85764, Germany; Joint Mass Spectrometry Center, Chair of Analytical Chemistry, University of Rostock, Rostock 18059, Germany*

Complete contact information is available at: https://pubs.acs.org/10.1021/acs.est.0c04776

Notes

The authors declare no competing financial interest.

■ ACKNOWLEDGMENTS

The work is funded by the Germany Federal Ministry of Transport and Digital Infrastructure (BMVI) as part of SmartAQnet (grant no.19F2003B), the Research Project of

the Ministry of Science and Technology of China (2019YFC0507800), the Support Project of High-Level Teachers in Beijing Municipal Universities in the Period of 13th Five-Year Plan (CIT&TCD201904037), and the China Scholarship Council (CSC) under the State Scholarship Fund (file no. 201706860028). We also gratefully thank Mr. Hadiatullah from Tianjin University for his deep discussion and review editing of our manuscript and Aethlabs (especially Drew Hill and Jeffrey Blair) for providing assistance with troubleshooting the MA200.

REFERENCES

(1) World Health Organization *Air quality guidelines: global update 2005: particulate matter, ozone, nitrogen dioxide, and sulfur dioxide*; World Health Organization: 2006.

(2) Qadir, R. M.; Schnelle-Kreis, J.; Abbaszade, G.; Arteaga-Salas, J. M.; Diemer, J.; Zimmermann, R. Spatial and temporal variability of source contributions to ambient PM10 during winter in Augsburg, Germany using organic and inorganic tracers. *Chemosphere* **2014**, *103*, 263−273.

(3) Wei, X.; Gao, B.; Wang, P.; Zhou, H.; Lu, J. Pollution characteristics and health risk assessment of heavy metals in street dusts from different functional areas in Beijing, China. *Ecotoxicol. Environ. Saf.* **2015**, *112*, 186−192.

(4) Putaud, J.-P.; Raes, F.; Van Dingenen, R.; Brüggemann, E.; Facchini, M.-C.; Decesari, S.; Fuzzi, S.; Gehrig, R.; Hüglin, C.; Laj, P.; Lorbeer, G.; Maenhaut, W.; Mihalopoulos, N.; Müller, K.; Querol, X.; Rodriguez, S.; Schneider, J.; Sprindler, G.; Brink, H. t.; Tørseth, K.; Wiedensohler, A. A European aerosol phenomenology—2: chemical characteristics of particulate matter at kerbside, urban, rural and background sites in Europe. *Atmos. Environ.* **2004**, *38*, 2579−2595.

(5) Kampa, M.; Castanas, E. Human health effects of air pollution. *Environ. Pollut.* **2008**, *151*, 362−367.

(6) Ye, B.; Ji, X.; Yang, H.; Yao, X.; Chan, C. K.; Cadle, S. H.; Chan, T.; Mulawa, P. A. Concentration and chemical composition of $PM_{2.5}$ in Shanghai for a 1-year period. *Atmos. Environ.* **2003**, *37*, 499−510.

(7) Cassee, F. R.; Héroux, M.-E.; Gerlofs-Nijland, M. E.; Kelly, F. J. Particulate matter beyond mass: recent health evidence on the role of fractions, chemical constituents and sources of emission. *Inhalation Toxicol.* **2013**, *25*, 802−812.

(8) IARC. Diesel and Gasoline Engine Exhausts and Some Nitroarenes. IARC Monographs on the Evaluation of Carcinogenic Risks to Humans. *IARC Monogr. Eval. Carcinog. Risks Hum.* **2014**, 9−699.

(9) Janssen, N. A. H.; Hoek, G.; Simic-Lawson, M.; Fischer, P.; Van Bree, L.; Brink, H. t.; Keuken, M.; Atkinson, R. W.; Anderson, H. R.; Brunekreef, B.; Cassee, F. R. Black carbon as an additional indicator of the adverse health effects of airborne particles compared with PM10 and PM2. 5. *Environ. Health Perspect.* **2011**, *119*, 1691−1699.

(10) Idso, C. D.; Idso, S. B.; Balling, R. C., Jr. The urban CO_2 dome of Phoenix, Arizona. *Phys. Geogr.* **2013**, *19*, 95−108.

(11) Brantley, H. L.; Hagler, G. S. W.; Kimbrough, E. S.; Williams, R. W.; Mukerjee, S.; Neas, L. M. Mobile air monitoring data-processing strategies and effects on spatial air pollution trends. *Atmos. Meas. Tech.* **2014**, *7*, 2169−2183.

(12) Kolb, C. E.; Herndon, S. C.; McManus, J. B.; Shorter, J. H.; Zahniser, M. S.; Nelson, D. D.; Jayne, J. T.; Canagaratna, M. R.; Worsnop, D. R. Mobile Laboratory with Rapid Response Instruments for Real-Time Measurements of Urban and Regional Trace Gas and Particulate Distributions and Emission Source Characteristics. *Environ. Sci. Technol.* **2004**, *38*, 5694−5703.

(13) Westerdahl, D.; Fruin, S.; Sax, T.; Fine, P. M.; Sioutas, C. Mobile platform measurements of ultrafine particles and associated pollutant concentrations on freeways and residential streets in Los Angeles. *Atmos. Environ.* **2005**, *39*, 3597−3610.

(14) Dons, E.; Panis, L. I.; Van Poppel, M.; Theunis, J.; Wets, G. Personal exposure to Black Carbon in transport microenvironments. *Atmos. Environ.* **2012**, *55*, 392−398.

(15) Pattinson, W.; Longley, I.; Kingham, S. Using mobile monitoring to visualise diurnal variation of traffic pollutants across two near-highway neighbourhoods. *Atmos. Environ.* **2014**, *94*, 782−792.

(16) Hankey, S.; Marshall, J. D. Land Use Regression Models of On-Road Particulate Air Pollution (Particle Number, Black Carbon, $PM_{2.5}$, Particle Size) Using Mobile Monitoring. *Environ. Sci. Technol.* **2015**, *49*, 9194−9202.

(17) Bassok, A.; Hurvitz, P. M.; Bae, C.-H. C.; Larson, T. Measuring neighbourhood air pollution: the case of Seattle's international district. *J. Environ. Plann. Manage.* **2010**, *53*, 23−39.

(18) Dons, E.; Temmerman, P.; Van Poppel, M.; Bellemans, T.; Wets, G.; Panis, L. I. Street characteristics and traffic factors determining road users' exposure to black carbon. *Sci. Total Environ.* **2013**, *447*, 72−79.

(19) Ragettli, M. S.; Corradi, E.; Braun-Fahrländer, C.; Schindler, C.; de Nazelle, A.; Jerrett, M.; Ducret-Stich, R. E.; Künzli, N.; Phuleria, H. C. Commuter exposure to ultrafine particles in different urban locations, transportation modes and routes. *Atmos. Environ.* **2013**, *77*, 376−384.

(20) Ghassoun, Y.; Ruths, M.; Löwner, M.-O.; Weber, S. Intra-urban variation of ultrafine particles as evaluated by process related land use and pollutant driven regression modelling. *Sci. Total Environ.* **2015**, *536*, 150−160.

(21) Klompmaker, J. O.; Montagne, D. R.; Meliefste, K.; Hoek, G.; Brunekreef, B. Spatial variation of ultrafine particles and black carbon in two cities: Results from a short-term measurement campaign. *Sci. Total Environ.* **2015**, *508*, 266−275.

(22) Choi, W.; Ranasinghe, D.; Bunavage, K.; DeShazo, J. R.; Wu, L.; Seguel, R.; Winer, A. M.; Paulson, S. E. The effects of the built environment, traffic patterns, and micrometeorology on street level ultrafine particle concentrations at a block scale: Results from multiple urban sites. *Sci. Total Environ.* **2016**, *553*, 474−485.

(23) Apte, J. S.; Messier, K. P.; Gani, S.; Brauer, M.; Kirchstetter, T. W.; Lunden, M. M.; Marshall, J. D.; Portier, C. J.; Vermeulen, R. C. H.; Hamburg, S. P. High-Resolution Air Pollution Mapping with Google Street View Cars: Exploiting Big Data. *Environ. Sci. Technol.* **2017**, *51*, 6999−7008.

(24) Messier, K. P.; Chambliss, S. E.; Gani, S.; Alvarez, R.; Brauer, M.; Choi, J. J.; Hamburg, S. P.; Kerckhoffs, J.; LaFranchi, B.; Lunden, M. M.; Marshall, J. D.; Portier, C. J.; Roy, A.; Szpiro, A. A.; Vermeulen, R. C. H.; Apte, J. S. Mapping Air Pollution with Google Street View Cars: Efficient Approaches with Mobile Monitoring and Land Use Regression. *Environ. Sci. Technol.* **2018**, *52*, 12563−12572.

(25) Hankey, S.; Marshall, J. D. On-bicycle exposure to particulate air pollution: Particle number, black carbon, PM2. 5, and particle size. *Atmos. Environ.* **2015**, *122*, 65−73.

(26) Liang, J.; Gong, J.; Sun, J.; Zhou, J.; Li, W.; Li, Y.; Liu, J.; Shen, S. Automatic sky view factor estimation from street view photographs—a big data approach. *Remote Sens.* **2017**, *9*, 411.

(27) Middel, A.; Lukasczyk, J.; Zakrzewski, S.; Arnold, M.; Maciejewski, R. Urban form and composition of street canyons: A human-centric big data and deep learning approach. *Landscape Urban. Plann.* **2019**, *183*, 122−132.

(28) Lack, D. A.; Langridge, J. M. On the attribution of black and brown carbon light absorption using the Ångström exponent. *Atmos. Chem. Phys.* **2013**, *13*, 10535−10543.

(29) Petzold, A.; Ogren, J. A.; Fiebig, M.; Laj, P.; Li, S.-M.; Baltensperger, U.; Holzer-Popp, T.; Kinne, S.; Pappalardo, G.; Sugimoto, N.; Wehrli, C.; Wiedensohler, A.; Zhang, X. Recommendations for reporting "black carbon" measurements. *Atmos. Chem. Phys.* **2013**, *13*, 8365−8379.

(30) Olson, M. R.; Victoria Garcia, M.; Robinson, M. A.; Van Rooy, P.; Dietenberger, M. A.; Bergin, M.; Schauer, J. J. Investigation of black and brown carbon multiple-wavelength-dependent light absorption from biomass and fossil fuel combustion source emissions. *J. Geophys. Res.: Atmos.* **2015**, *120*, 6682−6697.

https://dx.doi.org/10.1021/acs.est.0c04776
Environ. Sci. Technol. XXXX, XXX, XXX−XXX

(31) Feng, Y.; Ramanathan, V.; Kotamarthi, V. R. Brown carbon: a significant atmospheric absorber of solar radiation? *Atmos. Chem. Phys.* **2013**, *13*, 2795−2833.
(32) Pitz, M.; Birmili, W.; Schmid, O.; Peters, A.; Wichmann, H. E.; Cyrys, J. Quality control and quality assurance for particle size distribution measurements at an urban monitoring station in Augsburg, Germany. *J. Environ. Monit.* **2008**, *10*, 1017−1024.
(33) Hagler, G. S. W.; Yelverton, T. L. B.; Vedantham, R.; Hansen, A. D. A.; Turner, J. R. Post-processing Method to Reduce Noise while Preserving High Time Resolution in Aethalometer Real-time Black Carbon Data. *Aerosol Air Qual. Res.* **2011**, *11*, 539−546.
(34) Liu, X.; Schnelle-Kreis, J.; Zhang, X.; Bendl, J.; Khedr, M.; Jakobi, G.; Schloter-Hai, B.; Hovorka, J.; Zimmermann, R. Integration of air pollution data collected by mobile measurement to derive a preliminary spatiotemporal air pollution profile from two neighboring German-Czech border villages. *Sci. Total Environ.* **2020**, *722*, 137632.
(35) Popeangă, J.; Lungu, I. Forecasting Final Energy Consumption using the Centered Moving Average Method and Time Series Analysis. *Database Syst. J.* **2014**, *5*, 42−50.
(36) Wang, J.; Sun, K.; Cheng, T.; Jiang, B.; Deng, C.; Zhao, Y.; Liu, D.; Mu, Y.; Tan, M.; Wang, X.; Liu, W.; Xiao, B. Deep high-resolution representation learning for visual recognition. In *IEEE Transaction on Pattern Analysis Machine Intelligence*; IEEE: 2020, 1−15.
(37) Zhou, Z.; Siddiquee, M. M. R.; Tajbakhsh, N.; Liang, J. Unet++: A nested u-net architecture for medical image segmentation. In *Deep Learning in Medical Image Analysis and Multimodal Learning for Clinical Decision Support*; Springer: Cham, 2018, 3−11.
(38) He, K.; Zhang, X.; Ren, S.; Sun, J. Deep residual learning for image recognition. In *Proceedings of the IEEE Conference on Computer Vision and Pattern Recognition;* IEEE: 2016, 770−778.
(39) Chen, L. C.; Papandreou, G.; Schroff, F.; Adam, H. Rethinking atrous convolution for semantic image segmentation. *arXiv* preprint arXiv:1706.05587. **2017**.
(40) Chen, L.-C.; Zhu, Y.; Papandreou, G.; Schroff, F.; Adam, H. Encoder-decoder with atrous separable convolution for semantic image segmentation. In *Proceedings of the European conference on Computer Vision*; ECCV: 2018, 801−818.
(41) Zhao, H.; Zhang, Y.; Liu, S.; Shi, J.; Change Loy, C.; Lin, D.; Jia, J. Psanet: Point-wise spatial attention network for scene parsing. In *Proceedings of the European Conference on Computer Vision*; ECCV: 2018, 267−283.
(42) Xu, N.; Fisher, T. C.; Hong, J. Rademacher upper bounds for cross-validation errors with an application to the lasso. *arXiv* **2020**, 1−17
(43) Breiman, L. Bagging predictors. *Mach. Learn.* **1996**, *2*, 123−140.
(44) Ho, T. K. The random subspace method for constructing decision forests. In *IEEE Transactions on Pattern Analysis and Machine Intelligence*; IEEE: 1998, *20* (8), 832−844.
(45) Vapnik, V. N. An overview of statistical learning theory. In *IEEE Transactions on Neural Networks*; IEEE: 1999, *5* (10), 988−999.
(46) Mnih, V.; Heess, N.; Graves, A. Recurrent models of visual attention. In *Advances in Neural Information Processing Systems*; NIPS: 2014, 2204−2212.
(47) Peters, J.; Theunis, J.; Poppel, M. V.; Berghmans, P. Monitoring PM10 and Ultrafine Particles in Urban Environments Using Mobile Measurements. *Aerosol Air Qual. Res.* **2013**, *13*, 509−522.
(48) Targino, A. C.; Gibson, M. D.; Krecl, P.; Rodrigues, M. V. C.; dos Santos, M. M.; de Paula Corrêa, M. Hotspots of black carbon and $PM_{2.5}$ in an urban area and relationships to traffic characteristics. *Environ. Pollut.* **2016**, *218*, 475−486.
(49) Boogaard, H.; Kos, G. P. A.; Weijers, E. P.; Janssen, N. A. H.; Fischer, P. H.; van der Zee, S. C.; de Hartog, J. J.; Hoek, G. Contrast in air pollution components between major streets and background locations: Particulate matter mass, black carbon, elemental composition, nitrogen oxide and ultrafine particle number. *Atmos. Environ.* **2011**, *45*, 650−658.
(50) Pan, H.; Bartolome, C.; Gutierrez, E.; Princevac, M.; Edwards, R.; Boarnet, M. G.; Houston, D. Investigation of roadside fine particulate matter concentration surrounding major arterials in five Southern Californian cities. *J. Air Waste Manage. Assoc.* **2013**, *63*, 482−498.
(51) Wang, Y.; Xing, Z.; Zhao, S.; Zheng, M.; Mu, C.; Du, K. Are emissions of black carbon from gasoline vehicles overestimated? Real-time, in situ measurement of black carbon emission factors. *Sci. Total Environ.* **2016**, *547*, 422−428.
(52) Nguyen, T.; Yu, X.; Zhang, Z.; Liu, M.; Liu, X. Relationship between types of urban forest and $PM_{2.5}$ capture at three growth stages of leaves. *J. Environ. Sci.* **2015**, *27*, 33−41.
(53) Yassin, M. F. Impact of height and shape of building roof on air quality in urban street canyons. *Atmos. Environ.* **2011**, *45*, 5220−5229.
(54) Brokamp, C.; Jandarov, R.; Rao, M. B.; LeMasters, G.; Ryan, P. Exposure assessment models for elemental components of particulate matter in an urban environment: A comparison of regression and random forest approaches. *Atmos. Environ.* **2017**, *151*, 1−11.
(55) Brandt, C.; Kunde, R.; Dobmeier, B.; Schnelle-Kreis, J.; Orasche, J.; Schmoeckel, G.; Diemer, J.; Zimmermann, R.; Gaderer, M. Ambient PM_{10} concentrations from wood combustion−Emission modeling and dispersion calculation for the city area of Augsburg, Germany. *Atmos. Environ.* **2011**, *45*, 3466−3474.
(56) Jerrett, M.; Arain, A.; Kanaroglou, P.; Beckerman, B.; Potoglou, D.; Sahsuvaroglu, T.; Morrison, J.; Giovis, C. A review and evaluation of intraurban air pollution exposure models. *J. Exposure Sci. Environ. Epidemiol.* **2005**, *15*, 185−204.
(57) Holmes, N. S.; Morawska, L. A review of dispersion modelling and its application to the dispersion of particles: an overview of different dispersion models available. *Atmos. Environ.* **2006**, *40*, 5902−5928.
(58) Wolf, K.; Cyrys, J.; Harciníková, T.; Gu, J.; Kusch, T.; Hampel, R.; Schneider, A.; Peters, A. Land use regression modeling of ultrafine particles, ozone, nitrogen oxides and markers of particulate matter pollution in Augsburg, Germany. *Sci. Total Environ.* **2017**, *579*, 1531−1540.
(59) Tripathy, S.; Tunno, B. J.; Michanowicz, D. R.; Kinnee, E.; Shmool, J. L. C.; Gillooly, S.; Clougherty, J. E. Hybrid land use regression modeling for estimating spatio-temporal exposures to $PM_{2.5}$, BC, and metal components across a metropolitan area of complex terrain and industrial sources. *Sci. Total Environ.* **2019**, *673*, 54−63.
(60) Johnson, A. L.; Abramson, M. J.; Dennekamp, M.; Williamson, G. J.; Guo, Y. Particulate matter modelling techniques for epidemiological studies of open biomass fire smoke exposure: a review. *Air Qual., Atmos. Health* **2020**, *13*, 35−75.

https://dx.doi.org/10.1021/acs.est.0c04776
Environ. Sci. Technol. XXXX, XXX, XXX−XXX